Bonding Investigation of the Ground and Low-Lying States of the Titanium Boride Cation, TiB^+

Apostolos Kalemos and Aristides Mavridis*

Department of Chemistry, Laboratory of Physical Chemistry, National and Kapodistrian University of Athens, P.O. Box 64004, 15710 Zografou, Athens, Greece

Received: February 11, 1998; In Final Form: April 20, 1998

The titanium boride cation system, TiB^+, has been examined by ab initio MRCI (CASSCF+1+2) methods. In addition to the ground, $X^5\Delta$ state, 23 low-lying excited states are reported with symmetries $^{1,3}\Sigma^+$, $^{1,3,5}\Sigma^-$, $^{1,3,5}\Pi$, $^{1,3,5}\Delta$, $^{1,3,5}\Phi$, and $^{1,3,5}\Gamma$, spanning an energy range of 35 kcal/mol. All reported states are bound with respect to the *ground* state atoms $Ti^+(a^4F) + B(^2P)$, with binding energies ranging from 47.6 ($X^5\Delta$) to 13.8 ($2^3{}^1\Pi$) kcal/mol. The state with the highest *internal bond strength* (120 kcal/mol) and the shortest bond length (1.866 Å) is the first excited $^1\Sigma^+$ state, binding via a "genuinely" triple bond. For all states studied we report total energies, bond lengths, harmonic frequencies, and full potential energy curves, while an effort has been made to interpret bonding interactions by employing simple valence-bond diagrams.

1. Introduction

The challenging problems entailed in the ab initio electronic structure calculations of transition metal containing compounds are well-known.[1] They stem, mainly, from the high density of low-lying atomic states of the transition metal atom(s),[2] which in turn are due to the similarity of *n*d, (*n*+1)s, and (*n*+1)p orbitals both in spatial extension and energy.[3] The combining effect of low-lying high angular momentum (atomic) states gives rise to an extremely complex manifold of entangled molecular states with a variety of binding mechanisms. The importance of the transition metal containing molecular systems is reflected in the corresponding vast literature, experimental and/or theoretical.[4] It is indeed the purpose of this paper to examine by high-level ab initio techniques the binding modes and dissociation energies of a number of states of the diatomic molecule titanium boride, TiB^+. The present report can be considered as a continuation of our recent work on the ScB^+ system,[5] while work is in progress for the VB^+ and CrB^+ systems.

The states examined presently trace their origin to the a^4F and a^2F states of the Ti^+ cation and to the ^2P state of the B atom. The total number of states resulting from the asymptotic fragments are given by the product $|^{2S+1}L, M_L, M_S\rangle_{Ti^+} \otimes |^{2S+1}L, M_L, M_S\rangle_B$, or $Ti^+(a^4F, b^4F, a^2F) + B(^2P) \rightarrow$ 420 states of $|^{2S+1}\Lambda, M_S\rangle$ symmetry. Disregarding the M_S degeneracy, the 420 states collapse into the following 72, case (a) Hund states: $^1\Sigma^+$, $^1\Sigma^-(2)$, $^3\Sigma^+(3)$, $^3\Sigma^-(6)$, $^5\Sigma^+(2)$, $^5\Sigma^-(4)$, $^1\Pi(3)$, $^3\Pi(9)$, $^5\Pi(6)$, $^1\Delta(3)$, $^3\Delta(9)$, $^5\Delta(6)$, $^1\Phi(2)$, $^3\Phi(6)$, $^5\Phi(4)$, $^1\Gamma$, $^3\Gamma(3)$, and $^5\Gamma(2)$. Preliminary calculations at the CASSCF level were employed to select the first 23 out of the above 72 states, namely, $^1\Sigma^+$, $^1\Sigma^-$, $^3\Sigma^+$, $^3\Sigma^-$, $^5\Sigma^-$, $^1\Pi(3)$, $^3\Pi$, $^5\Pi$, $^1\Delta(2)$, $^3\Delta(2)$, $^5\Delta(2)$, $^1\Phi(2)$, $^3\Phi$, $^5\Phi$, $^1\Gamma$, $^3\Gamma$, and $^5\Gamma$. An additional state of $^1\Sigma^+$ symmetry has been calculated correlating to $Ti^+(a^2D; M=0) + B(^2P; M=0)$ fragments. For these 24 states full potential energy curves (PEC) were constructed at the multireference configuration interaction level (MRCISD = CASSCF + single + double replacements). Henceforth and for all states examined we report total energies, dissociation energies, equilibrium bond distances, harmonic frequencies, and energy gaps.

2. Computational Approach

For the Ti atom the ANO basis set 21s16p9d6f4g of Bauschlicher[6] was selected but with the functions of g symmetry removed. This set was generalized contracted to 7s6p4d3f. For the B atom the correlation consistent basis set cc-pVTZ 10s5p2d1f of Dunning[7] was used, contracted to 4s3p2d1f. The resulting contracted basis set space contains 96 spherical Gaussian functions (5d and 7f functions).

As was already mentioned, the complete active space SCF + single + double replacements = MRCI method was used, perhaps the only practical method available that is variational and, due to the relatively small number of active electrons, essentially size consistent and size extensive[8,9] (vide infra).

The (reference) CAS space selected is composed of 10 orbital functions, six of which correspond asymptotically to the valence-occupied space of $Ti^+(4s+3d)$, and the rest to the valence space of the B atom (2s+2p). The number of configuration functions (CFs) ensuing from distributing six electrons among 10 orbitals ranges from about 600 to 1700 CFs according to the symmetry of the state. Although all our calculations were performed under C_{2v} symmetry restrictions, the CASSCF wave functions display axial angular momentum symmetry, viz., $|\Lambda| = 0$, 1, 2, 3, and 4 or $\Sigma^\pm$, Π, Δ, Φ, and Γ, respectively.

Valence correlation energy was extracted by single and double excitations out of the reference CAS space (MRCI). To keep the computations under control, the approach of "internal contraction" was also employed (icMRCI);[10] thus our largest CI expansion did not exceed the number of half a million CFs.

Due to the involved nature of the PECs, we were forced to use the state-average (SA) technique.[11,12] Numerical experiments for the ground ($X^5\Delta$) and for the first excited ($1^1\Sigma^+$) state performed with and without the SA method showed total energy losses of 0.6 and 1.2 mhartrees and differences in bond lengths of 0.004 and 0.015 Å, respectively, with the SA bond distances always being longer. Energy losses of about 1 mhartree were also found due to the internal contraction methodology employed here. Judging as adequate the basis set functional space, no superposition effects were taken into account.

S1089-5639(98)01088-3 CCC: $15.00
Published on Web 06/19/1998

TABLE 1: Total Energies of the a^4F, b^4F, a^2F and b^2D Ti^+ States and of the ^2P and ^4P States of B Atom in Different Methodologies

	Ti^+			
method	a^4F	b^4F	a^2F	b^2D
NHF[a]	−848.203 401			
SCF	−848.205 050	−848.188 433	−848.178 839	
CISD	−848.219 503	−848.214 373	−848.200 178	
sa-SCF[b]	−848.202 973	−848.186 613	−848.176 882	−848.146 098
CISD	−848.217 562	−848.212 684	−848.198 192	−848.173 758

	B	
method	^2P	^4P
NHF[c]	−24.529 061	
SCF	−24.528 147	−24.451 286
CISD	−24.596 634	−24.467 237
sa-CASSCF[b]	−24.559 329	
MRCISD	−24.598 396	

[a] Numerical Hartree−Fock, ref 15b. [b] Spherically averaged SCF or CASSCF. [c] Numerical HF, ref 16.

All calculations were done with the MOLPRO suite of codes;[13] some test calculations were also done with the COLUMBUS[14] code.

3. The Atoms

The spherically averaged SCF energy of the Ti ground $^3F(4s^2-3d^2)$ state is −848.4057 76 hartrees, 0.40 mhartree higher than the numerical result,[15a] with corresponding CISD value of −848.458 670 hartree. Table 1 reports total energies of the Ti^+ $a^4F(4s3d^2)$, $b^4F(d^3)$, $a^2F(4s3d^2)$, and $b^2D(4s3d^2)$ states, as well as for the $^2P(2s^22p)$ and $^4P(2s2p^2)$ states of the B atom in different methodologies. Notice the +1.65 mhartrees energy difference between the numerical HF and our SCF of the Ti^+ system due to the contaminated angular momentum (spatial polarization) of the SCF vectors.[17] This symmetry contamination is removed at the spherically averaged SCF, with the energy at this level being 0.43 mhartree *higher* than the numerical value. From Table 1 it is seen that the Ti^+ atomic energy separations $b^4F \leftarrow a^4F$, $a^2F \leftarrow b^4F$, $b^2D \leftarrow a^2F$ at the CISD (spherically averaged) level are 0.132, 0.394, and 0.665 eV respectively, as compared to the corresponding experimental (average over M_J) values[2] of 0.107, 0.458, and 0.490 eV. For the B atom the calculated energy splitting $^4P \leftarrow {}^2P$ of 3.569 eV is in excellent agreement with the experimental number of 3.571 eV.[2] The not so good agreement between the experimental and calculated values of the metal cation splittings can be attributed to core−valence interaction correlation effects.

4. Results and Discussion

Tables 2, 3, and 4 present total energies (E), bond lengths (R_e), dissociation energies (D_e), harmonic frequencies (ω_e), and energy gaps (T_e) of the six quintets, seven triplets, and 11 singlets of $\Sigma^{\pm}$, Π, Δ, Φ, and Γ spatial symmetry, at the CASSCF, icMRCI, and icMRCI+Q (icMRCI + multireference Davidson correction[18]) methods. An overall picture of the 24 PECs morphology is shown in Figure 1, while Figure 2 presents a level state diagram; notice that the energy range in which all 24 states are embedded is 1.5 eV, with some of the states differing by less than 1 mhartree. Numbers in front of the state symbols refer to absolute energy ordering with respect to the ground-X state.

In the discussion that follows the quintets are presented first, followed by the triplets and finally by the singlets.

TABLE 2: Energies E (hartree), Bond Distances R_e (Å), Dissociation Energies D_e (kcal/mol), Harmonic Frequencies ω_e (cm^{-1}), and Energy Gaps T_e (kcal/mol) of the $X^5\Delta$, $3^5\Phi$, $4^5\Sigma^-$, $7^5\Pi$, $19^5\Delta$, and $22^5\Gamma$ States of TiB^+ in Ascending Energy Order

state	method[a,b]	$-E$	R_e	D_e	ω_e	T_e[c]
$X^5\Delta$	CASSCF	872.812 17	2.121	31.1	528	0.0
	icMRCISD	872.891 34	2.102	47.6	519	0.0
	icMRCI+Q	872.8957	2.104	49.0	507	0.0
$3^5\Phi$	CASSCF	872.797 74	2.346	20.0	400	9.1
	icMRCISD	872.868 18	2.344	33.0	414	14.5
	icMRCI+Q	872.8720	2.345	34.3	417	14.9
$4^5\Sigma^-$	CASSCF	872.793 84	2.219	18.6	392	11.5
	icMRCISD	872.867 40	2.210	32.2	445	15.0
	icMRCI+Q	872.8715	2.218	33.5	437	15.2
$7^5\Pi$	CASSCF	872.792 09	2.338	16.7	442	12.6
	icMRCISD	872.863 34	2.345	30.2	417	17.6
	icMRCI+Q	872.8673	2.346	31.6	413	17.8
$19^5\Delta$	CASSCF	872.768 15	2.223	3.7	504	27.6
	icMRCISD	872.845 99	2.185	19.4	527	28.5
	icMRCI+Q	872.8505	2.186	21.0	527	28.3
$22^5\Gamma$	icMRCISD	872.836 82	2.384	13.7	262	34.2
	icMRCI+Q	872.8441	2.371	17.0	343	32.4

[a] The CASSCF results have been obtained by the state-average method. [b] $+Q$ refers to the multireference Davidson correction, ref 18. [c] 1 hartree = 627.51 kcal/mol.

4.1. Quintets. *Ground, $X^5\Delta$ State.* At equilibrium the leading configuration (A_1 component) is given by, $X|^5\Delta\rangle \sim 1\sigma^2 (\sim 2s_B^2)2\sigma^1 1\pi_x^1 1\pi_y^1 1\delta^1_-$, or in terms of the asymptotic fragments $X|^5\Delta\rangle = |a^4F;\ M = \pm 2\rangle \otimes |^2P;\ M = 0\rangle$. Schematically, the binding interaction can be represented by the valence-bond-Lewis (vbL) icon

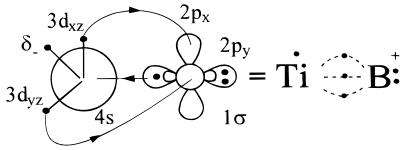

which suggests that the two atoms are held together by two half π bonds originating from the metal cation and a half σ bond originating from the B atom. The δ_- orbital has a pure 3d character with no participation in the binding mechanism; in essence, the δ_- is a spectator electron carrying the $|\Lambda| = 2$ symmetry. The situation here is in striking similarity to the ground $^4\Sigma^-$ state of the ScB^+ system,[5] and this is clearly reflected in the numerical results: from Table 2 we see that the D_e, R_e, and ω_e values of TiB^+ are 47.6 kcal/mol, 2.102 Å, and 519 cm^{-1}, as compared to 44.9 kcal/mol, 2.160 Å, and 513 cm^{-1} of the ScB^+ species at the MRCI level. At equilibrium the CAS atomic populations are (first entry Ti, second entry B)

$$4s^{0.25}4p_z^{0.08}3d_{z^2}^{0.44}3d_{xz}^{0.60}3d_{yz}^{0.60}3d_{xy}^{1.0}/2s^{1.57}2p_z^{0.63}2p_x^{0.38}2p_y^{0.38}$$

giving full support of the previously reported vbL icon. The population analysis suggests that ~0.8 e^- are transferred from the B atom to the Ti atom via the σ frame, with a concomitant transfer of ~0.8 e^- from the Ti to the B atom via the π frame. In addition, the in situ metal finds itself in an excited $\sim d^3(b^4F;\ M=\pm 2)$ configuration, but the PEC (Figure 3) ends up in the a^4F state of the Ti^+ cation due to an avoided crossing around 6 bohr between two $^5\Delta$ states: the ground and the one originating from the b^4F state of the Ti^+. This was confirmed by constructing the $X^5\Delta$ PEC in two ways, with and without state average (SA): the SA-PEC among the first three $^5\Delta$ states (weighting vector, $w = 0.8, 0.1, 0.1$) results in the PEC shown in Figure 3, while the without-SA PEC results in the $b^4F(d^3)$

TABLE 3: Energies E (hartree), Bond Distances R_e (Å), Dissociation Energies D_e (kcal/mol), Harmonic Frequencies ω_e (cm^{-1}), and Energy Gaps T_e (kcal/mol) of the $2^3\Pi$, $5^3\Delta$, $6^3\Gamma$, $8^3\Sigma^-$, $10^3\Phi$, $11^3\Sigma^+$, and $12^3\Delta$ States of TiB^+ in Ascending Energy Order

state[a]	method[b,c]	$-E$	R_e	D_e	ω_e	T_e
$2^3\Pi_g$	CASSCF	872.794 63	1.945	20.0	616	11.0
	icMRCISD	872.873 68	1.953	36.6	578	11.1
	icMRCI+Q	872.8775	1.959	37.8	562	11.4
$2^3\Pi_l$	CASSCF	872.795 28	2.849	20.4	192	
	icMRCISD	872.859 52	2.711	27.8	276	
	icMRCI+Q	872.8629	2.672	28.6	236	
$5^3\Delta_g$	CASSCF	872.790 63	2.170	17.6	499	13.5
	icMRCISD	872.867 19	2.168	32.4	506	15.2
	icMRCI+Q	872.8717	2.172	34.0	483	15.1
$5^3\Delta_l$	CASSCF	872.794 03	2.896	19.7	278	
	icMRCISD	872.858 92	2.749	27.2	291	
	icMRCI+Q	872.8627	2.741	28.3	287	
$6^3\Gamma$	CASSCF	872.786 13	2.144	15.0	521	16.3
	icMRCISD	872.864 54	2.141	31.0	530	16.8
	icMRCI+Q	872.8682	2.145	32.0	494	17.3
$8^3\Sigma^-_g$	CASSCF	872.818 64	2.836	26.3	255	4.1
	icMRCISD	872.862 11	2.686	28.7	282	18.3
	icMRCI+Q	872.8648	2.665	29.3	282	19.4
$8^3\Sigma^-_l$	CASSCF	872.781 96	2.011			
	icMRCISD	872.858 54	2.011			
	icMRCI+Q	872.8623	2.011			
$10^3\Phi_g$	CASSCF	872.797 51	2.807	21.9	320	9.2
	icMRCISD	872.861 88	2.688	29.3	283	18.5
	icMRCI+Q	872.8654	2.690	30.3	284	19.0
$10^3\Phi_l$	CASSCF	872.780 06	2.033	10.9	503	
	icMRCISD	872.860 02	2.025	28.1	538	
	icMRCI+Q	872.8648	2.032	29.9	519	
$11^3\Sigma^+$	CASSCF	872.780 05	2.162	11.2	493	20.2
	icMRCISD	872.861 56	2.150	29.1	495	18.7
	icMRCI+Q	872.8671	2.155	31.3	497	18.0
$12^3\Delta_g$	CASSCF	872.782 40	2.093	12.7	533	18.7
	icMRCISD	872.861 25	2.108	29.0	448	18.9
	icMRCI+Q	872.8669	2.137	31.3	436	18.1
$12^3\Delta_l$	CASSCF	872.776 73	2.434	9.1		
	icMRCISD	872.854 50	2.493	24.7		
	icMRCI+Q	872.8598	2.532	26.8		

[a] "*g*" and "*l*" refer to "global" and "local" minimum, respectively; see text. [b] The CASSCF results have been obtained by the state-average method. [c] $+Q$ refers to the multireference Davidson correction, ref 18.

TABLE 4: Energies E (hartree), Bond Distances R_e (Å), Dissociation Energies D_e (kcal/mol), Harmonic Frequencies ω_e (cm^{-1}), and Energy Gaps T_e (kcal/mol) of the $1^1\Sigma^+$, $9^1\Pi$, $13^1\Gamma$, $14^1\Sigma^+$, $15^1\Delta$, $16^1\Phi$, $17^1\Delta$, $18^1\Pi$, $20^1\Sigma^-$, $21^1\Phi$, and $23^1\Pi$ States of TiB^+ in Ascending Energy Order

state[a]	method[b,c]	$-E$	R_e	D_e[d]	ω_e	T_e
$1^1\Sigma^+$	CASSCF	872.815 69	1.856	48.9	848	2.2
	icMRCISD	872.878 03	1.866	51.7	728	8.4
	icMRCI+Q	872.8811	1.875	51.9	714	9.2
$9^1\Pi$	CASSCF	872.782 03	1.990	28.4	550	18.9
	icMRCISD	872.862 09	1.993	41.7	534	18.4
	icMRCI+Q	872.8663	2.003	42.6	512	18.4
$13^1\Gamma$	CASSCF	872.780 47	2.215	27.1	525	19.9
	icMRCISD	872.857 67	2.204	38.8	524	21.1
	icMRCI+Q	872.8621	2.208	40.0	524	21.1
$14^1\Sigma^+$	CASSCF	872.776 82	2.086	44.8	721	22.2
	icMRCISD	872.85636	2.093	52.8	722	22.0
	icMRCI+Q	872.8601	2.096	55.2	678	22.3
$15^1\Delta$	CASSCF	872.775 12	2.181	23.7	463	23.3
	icMRCISD	872.854 43	2.180	36.8	475	23.2
	icMRCI+Q	872.8585	2.185	37.6	481	23.4
$16^1\Phi$	CASSCF	872.768 23	2.011	19.9	608	27.6
	icMRCISD	872.850 74	2.010	34.7	592	25.5
	icMRCI+Q	872.8551	2.020	35.7	673	25.5
$17^1\Delta$	CASSCF	872.766 64	2.135	18.6	459	28.6
	icMRCISD	872.847 61	2.131	32.7	476	27.4
	icMRCI+Q	872.8516	2.147	35.2	436	27.7
$18^1\Pi$	CASSCF	872.765 04	2.236	18.1	468	29.6
	icMRCISD	872.846 49	2.230	31.8	473	28.1
	icMRCI+Q	872.8514	2.231	33.1	513	27.8
$20^1\Sigma^-$	CASSCF	872.761 85	2.230	14.8	499	31.6
	icMRCISD	872.845 55	2.205	30.8	542	28.7
	icMRCI+Q	872.8525	2.206	33.4	551	27.1
$21^1\Phi$	CASSCF	872.759 91	2.184	14.9	828	32.8
	icMRCISD	872.839 43	2.207	27.4	765	32.6
	icMRCI+Q	872.8446	2.210	28.8	760	32.1
$23^1\Pi_g$	CASSCF	872.751 83	2.132	10.1	595	37.9
	icMRCISD	872.836 61	2.109	25.9	531	34.3
	icMRCI+Q	872.8423	2.117	27.7	542	33.5
$23^1\Pi_l$	CASSCF	872.747 15	2.646	7.2		
	icMRCISD	872.825 50	2.559	18.9		
	icMRCI+Q	872.8309	2.548	20.5		

[a] "*g*" and "*l*" refer to "global" and "local" minimum, respectively; see text. [b] The CASSCF results have been obtained by the state-average method. [c] $+Q$ refers to the multireference Davidson correction, ref 18. [d] D_e is with respect to the adiabatic products.

state of the metal, an effect due to the instability of the MCSCF and/or MRCI equations.

$3^5\Phi$ State (2nd of the Quintets). At equilibrium the leading terms (B_1 component) are, $3|^5\Phi\rangle \sim |1\sigma^2 2\sigma^1 3\sigma^1 1\delta^1_+ 1\pi^1_x\rangle + |1\sigma^2 2\sigma^1 3\sigma^1 1\pi^1_y 1\delta^1_-\rangle$, with the asymptotic representation given by the product

$$3|^5\Phi\rangle = |a^4F;\, M = \pm 3\rangle \otimes |^2P;\, M = 0\rangle$$

The binding mode can be represented by the superposition of two vbL pictures,

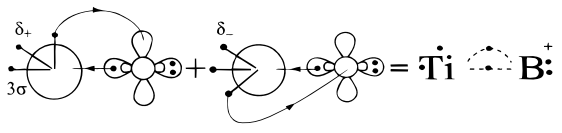

with a half σ bond, a half π bond, and a spectator e^- of $\delta_\pm$ symmetry. The CAS atomic populations are

$$4s^{0.69}4p_z^{0.07}3d_{z^2}^{0.89}3d_{xz}^{0.23}3d_{yz}^{0.23}3d_{x^2-y^2}^{0.50}3d_{xy}^{0.50}/2s^{1.66}2p_z^{0.63}2p_x^{0.26}2p_y^{0.26}$$

in agreement with the vbL icon. At infinity we start with a d distribution of $3d_{xz}^{0.50}3d_{yz}^{0.50}$, resulting in $3d_{xz}^{0.23}3d_{yz}^{0.23}$ at equilibrium, while 0.52 e^- are tranferred to the $2p_x$, $2p_y$ boron orbitals, resulting in the half π bond. In the σ frame ~1 e^- is distributed to the 3σ orbital, with the $3d_{z^2}(0.89) + 4p_z(0.07)$ Ti populations steming from the B σ frame ($0.7 = 3 - 1.66 - 0.63$), plus 0.3 e^- from the Ti 4s orbital. Finally, the $\delta_\pm$ electron maintains its integrity along the whole of the PEC, Figure 3. Overall a transfer of 0.15 e^- occurs from the B to the Ti atom. From

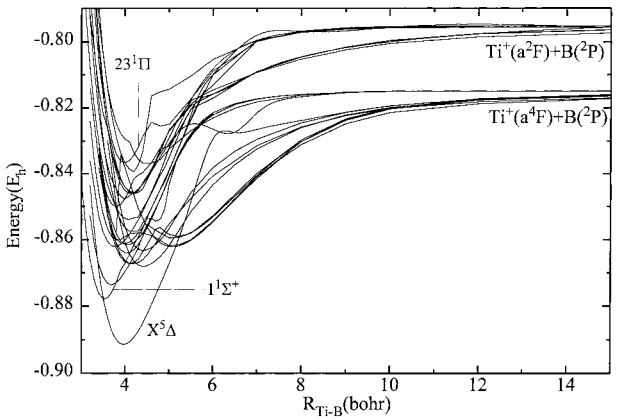

Figure 1. MRCI potential energy curves of all 24 TiB^+ states examined in the present paper.

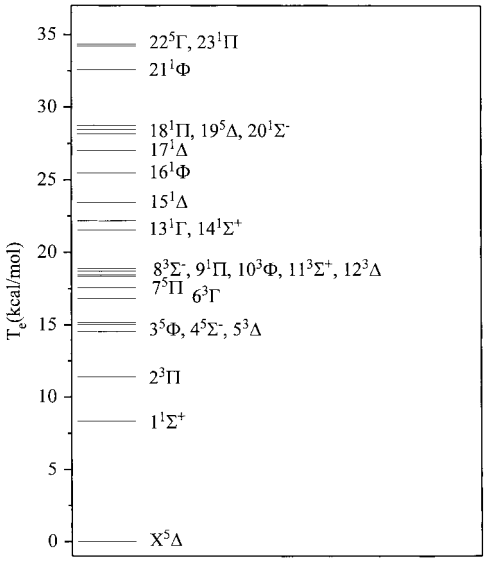

Figure 2. Relative energy level diagram of the TiB^+ system.

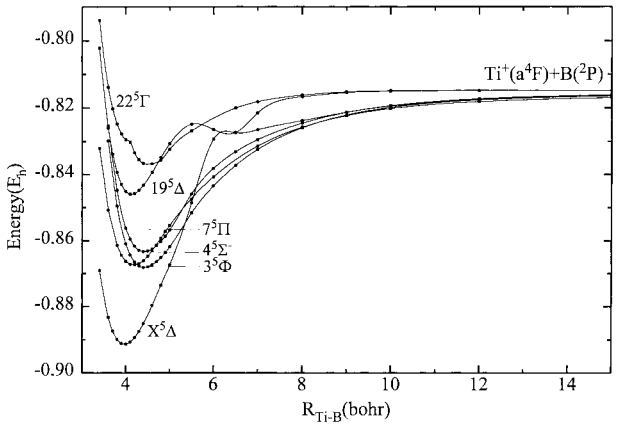

Figure 3. Potential energy curves of six quintet states; MRCI level of theory.

Table 2 we see that the D_e and R_e values are 33 kcal/mol and 2.344 Å at the MRCI level, the latter value being longer by 0.24 Å as compared to the $X^5\Delta$ state, consistent with the reduction of bonding order by a half π bond from the $X^5\Delta$ to the $3^5\Phi$ state.

$4^5\Sigma^-$ State (3rd of the Quintets). At equilibrium the leading configurations of the $4^5\Sigma^-$ are

$$4|^5\Sigma^-\rangle \sim 0.88|1\sigma^2 2\sigma^1 3\sigma^1 1\pi_x^1 1\pi_y^1\rangle - 0.22|1\sigma^2 2\sigma^1 3\sigma^1 1\delta_+^1 1\delta_-^1\rangle$$

in essence differing from the $X^5\Delta$ state by an orbital interchange, δ_- to 3σ. Asymptotically, we have the product $4|^5\Sigma^-\rangle = |a^4F; M = 0\rangle \otimes |^2P; M = 0\rangle$. The binding scheme is very similar to that of the $X^5\Delta$ state with the following vbL picture:

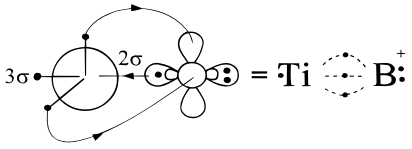

with two half π bonds and one half σ bond. The CAS atomic populations

$$4s^{0.81}4p_z^{0.06}3d_{z^2}^{0.74}3d_{xz}^{0.72}3d_{yz}^{0.72}3d_{x^2-y^2}^{0.07}3d_{xy}^{0.07}/2s^{1.66}2p_z^{0.65}2p_x^{0.24}2p_y^{0.24}$$

corroborate the above bonding mode. In the π frame approximately 0.5 e^- is transferred from the metal to the B atom, with a synchronous migration of $\sim$ 0.7 e^- from the B to the Ti atom via the σ frame. As a result, the B atom is losing $\sim$0.2 e^- toward the metal.

In every respect this state is similar to the $2^4\Sigma^-$ state of the ScB^+ molecule:[5] the binding mode between the two states is identical, while the numerical results are in practical agreement with D_e(*internal bond strength*) = 34.9 kcal/mol, R_e = 2.168 Å for the ScB^+, as compared to D_e = 32.2 kcal/mol and R_e = 2.210 Å of the TiB^+ (Table 2), at the MRCI level.

$7^5\Pi$ State (4th of the Quintets). The difference between this state and the previously reported $3|^5\Phi\rangle$ state is a sign flip between the two leading configurations, namely, $7|^5\Pi(^5B_1)\rangle \sim |1\sigma^2 2\sigma^1 3\sigma^1 1\delta_+^1 1\pi_x^1\rangle - |1\sigma^2 2\sigma^1 3\sigma^1 1\pi_y^1 1\delta_-^1\rangle$, with the asymptotic fragments described by the product wave function $7|^5\Pi\rangle = |a^4F; M = \pm 1\rangle \otimes |^2P; M = 0\rangle$. From Figure 3 we observe that the $3|^5\Phi\rangle$ and $7|^5\Pi\rangle$ PECs are "parallel", with Table 2 revealing the close agreement between the corresponding numerical findings.

$19^5\Delta$ State (5th of the Quintets). The leading configurations are

$$19|^5\Delta(^5A_1)\rangle \sim 0.86|1\sigma^2 2\sigma^1 1\pi_x^1 1\pi_y^1 1\delta_-^1\rangle - 0.16|1\sigma^1 2\sigma^1 3\bar{\sigma}^1 1\pi_x^1 1\pi_y^1 1\delta_-^1\rangle$$

while asymptotically we have $19|^5\Delta\rangle = |a^4F; M = \pm 3\rangle \otimes |^2P; M = \mp 1\rangle$. The CAS equilibrium atomic populations are

$$4s^{0.55}4p_z^{0.06}3d_{z^2}^{0.64}3d_{xz}^{0.45}3d_{yz}^{0.45}3d_{xy}^{1.0}/2s^{1.64}2p_z^{0.11}2p_x^{0.53}2p_y^{0.53}$$

suggesting the following vbL icon for the bonding interaction:

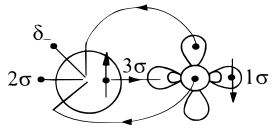

In this case an analysis of the σ orbitals is in order $2\sigma \sim 0.6(4s) - 0.8(3d_\sigma)$, $3\sigma \sim \{[0.5(4s) + 0.3(3d_\sigma)]_{Ti} - [0.5(2s) + 0.7(2p_\sigma)]_B\}$ with the 2σ "hybrid" localized on the metal and the 3σ clearly being the σ bond. The $19^5\Delta$ PEC shown in Figure 3 presents an avoided crossing around 5 bohr, due to the interaction of another $^5\Delta$ state originating from the first excited $^4P(2s2p^2)$ state of the B atom. This is also evident from the equilibrium electron distribution reported above: the in situ B atom finds itself in its ^4P, $M = 0$ projection, thus giving rise to two half π bonds with a transfer of $\sim$0.90 e^- from B to Ti; the half σ bond stems from the $M = \pm 2$ ($M = \pm 3$ at infinity) of the metal cation with the transfer of 0.75 e^- from Ti to B.

$22^5\Gamma$ State (6th of the Quintets). This is the last of the quintets, lying 34.2 kcal/mol above the the $X^5\Delta$ state, with a binding energy of 13.7(17) kcal/mol at the MRCI(+Q) level, Table 2. The twice as large difference between the MRCI and MRCI+Q D_e's of this state and the rest of the quintets is attributed to the nonoptimal character of the one-particle molecular basis set. This state was obtained as the third root of the MRCI matrix of $^5A_1$ symmetry. The leading equilibrium configurations are

$$22|^5\Gamma(^5A_1)\rangle \sim (|1\sigma^2 2\sigma^1 1\delta_+^1 1\pi_x^1 2\pi_x^1\rangle - |1\sigma^2 2\sigma^1 1\delta_+^1 1\pi_y^1 2\pi_y^1\rangle) + (|1\sigma^2 2\sigma^1 2\pi_x^1 1\pi_y^1 1\delta_-^1\rangle - |1\sigma^2 2\sigma^1 1\pi_x^1 2\pi_y^1 1\delta_-^1\rangle)$$

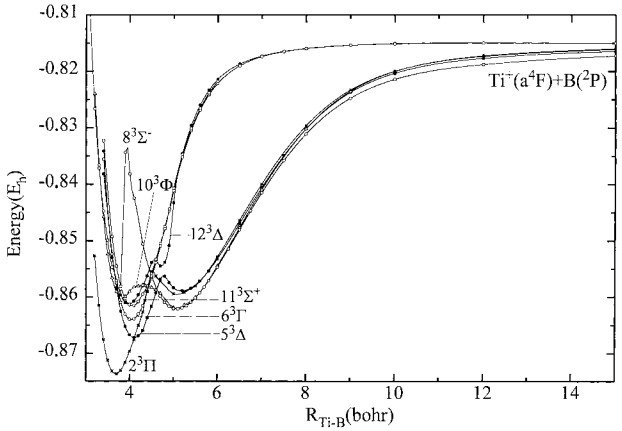

Figure 4. Potential energy curves of the triplet manifold; MRCI level of theory.

with the asymptotic wave function $22|^5\Gamma\rangle = |a^4F; M = \pm 3\rangle \otimes |^2P; M = \pm 1\rangle$. Visualizing the equilibrium configurations with the aid of the vbL diagrams, we obtain

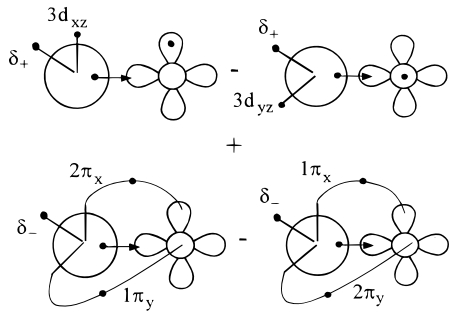

with $2\sigma \sim 0.6(4s) + 0.3(3d_\sigma) - 0.5(2s)$, $1\pi \sim 0.7(3d_\pi) + 0.6(2p_\pi)$, $2\pi \sim 0.7(3d_\pi) - 0.7(2p_\pi)$. The above vbL picture shows the difficulty of describing the chemical bonding process in a conventional manner.

4.2. Triplets. We report seven triplet states the PECs of which are shown in Figure 4; numerical results are presented in Table 3.

$2^3\Pi$ State (1st of the Triplets). The $2^3\Pi$ PEC presented in Figure 4 shows two minima, a "local" (*l*) around 5.1 bohr and a "global" (*g*) around 3.7 bohr, due to the interaction among three PECs asymptotically described by the fragments $|^3\Pi\rangle = |a^4F; M = \pm 1, \pm 2, 0\rangle \otimes |^2P; M = 0, \mp 1, \pm 1\rangle$. At the MRCI level, only the $|M = \pm 1\rangle \otimes |M = 0\rangle$ PEC has been constructed (Figure 4). At the "*l*" minimum the leading configurations are

$$2|^3\Pi(^3B_1)\rangle_1 \sim 0.43(|1\sigma^2 2\sigma^2 1\pi_y^1 1\delta_-^1\rangle - |1\sigma^2 2\sigma^2 1\delta_+^1 1\pi_x^1\rangle) + 0.40|1\sigma^2 2\sigma^2 3\sigma^1 1\pi_x^1\rangle$$

The CAS atomic populations at the "*l*" min are

$$4s^{1.08}4p_z^{0.07}3d_{z^2}^{0.40}3d_{xz}^{0.67}3d_{yz}^{0.33}3d_{x^2-y^2}^{0.33}3d_{xy}^{0.33}/2s^{1.84}2p_z^{0.84}2p_x^{0.06}2p_y^{0.06}$$

and entirely reflect the Ti^+ cation representation at infinity:

$$Ti^+(a^4F; M = \pm 1) = \sqrt{4/10}|4s^1 3d_{z^2}^1 3d_{xz}^1\rangle - \sqrt{3/10}|4s^1 3d_{xz}^1 3d_{x^2-y^2}^1\rangle + \sqrt{3/10}|4s^1 3d_{yz}^1 3d_{xy}^1\rangle$$

Indeed, the 0.67 e^- population of $3d_{xz}$, $(\sqrt{4/10})^2 + (\sqrt{3/10})^2$, plus the 0.33 e^- of d_{yz}, $(\sqrt{3/10})^2$, sum to 1.0 d_π e^-, indifferent to the bond, with a second spectator d e^- distributed to the $3d_{z^2}$-(0.40), $3d_{x^2-y^2}$(0.33), and $3d_{xy}$(0.33) orbitals, in accordance with the asymptotic coefficients $(\sqrt{4/10})^2$, $(\sqrt{3/10})^2$, and $(\sqrt{3/10})^2$, respectively. The two atoms are held together by a pure σ bond, while 0.20 e^- is transferred from the B to the Ti atom. The following vbL icon succinctly summarizes the bonding mode,

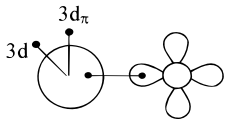

From Table 3 we see that the energy value of this σ bond amounts to 27.8 kcal/mol at the MRCI level at $R_e = 2.711$ Å. Essentially the same binding energies and bond distances are observed in all triplets where the binding is caused by a single σ bond (vide infra), i.e., $5^3\Delta_l$ (27.2 kcal/mol, 2.749 Å), $8^3\Sigma^-_g$ (28.7 kcal/mol, 2.686 Å), and $10^3\Phi_g$ (29.3 kcal/mol, 2.688 Å), Table 3.

It is interesting to note that the $3d_\pi$ (spectator) electron does not "diffuse" into the $2p_\pi$ empty orbital of the B atom. Perhaps the reason is that this electron results from the $0.67d_{xz} + 0.33d_{yz}$ distribution, dictated by the symmetry of the Ti^+ atom (a^4F; M=±1) alone, which is responsible for the molecular symmetry, the B atom always being in its $M = 0$ projection. In other words, an electron redistribution would change drastically the $(\sqrt{4/10}, \sqrt{3/10}, \sqrt{3/10})$ vector with a concomitant change of the $3d_{z^2}$ and $3d_{x^2-y^2}$, $3d_{xy}$ populations and finally to an energy gain and/or to a symmetry contamination.

At the "*g*" minimum the leading configurations are

$$2|^3\Pi(^3B_1)\rangle_g \sim 0.84|1\sigma^2 2\sigma^1 1\pi_x^1 1\pi_y^2\rangle + 0.19\{|1\sigma^2 1\pi_x^2 1\pi_y^1 1\delta_-^1\rangle - |1\sigma^2 1\delta_+^1 1\pi_x^1 1\pi_y^2\rangle\}$$

which, *diabatically*, correlates to the $|b^4F; M = 0\rangle \otimes |^2P; M = \pm 1\rangle$, with a switch of *M* values as compared to the "*l*" minimum. The CAS atomic populations are

$$4s^{0.21}4p_z^{0.11}3d_{z^2}^{0.70}3d_{xz}^{0.66}3d_{yz}^{1.18}3d_{x^2-y^2}^{0.08}3d_{xy}^{0.08}/2s^{1.52}2p_z^{0.36}2p_x^{0.35}2p_y^{0.67}$$

The binding scheme can be represented by the following vbL diagram.

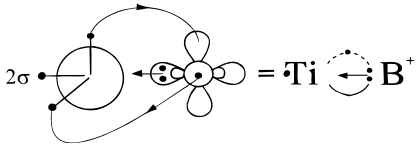

where $2s \sim 0.70(3d_{z^2}) - [0.20(2s) + 0.70(2p_z)]_B$. The bonding is due to a π bond (2 e^- distributed in the π_y frame ~1.18 + 0.67) and a half π bond (1 e^- distributed in the π_x frame ~0.66 + 0.35). Also, a strong hybridization between the 2s and $2p_z$ boron orbitals occurs, giving rise to a putative σ bond, while the in situ Ti atom appears to be by about 70% in a $d^3(b^4F)$ configuration, the rest being in its $4s3d^2(a^4F)$ configuration. Notice the very large 0.76 Å difference in bond length between the "*g*" and "*l*" minima. No charge transfer is observed.

$5^3\Delta$ State (2nd of the Triplets). The two minima shown in Figure 4 of this $5^3\Delta$ PEC, a local "*l*" and a global "*g*" around 5.2 and 4.1 bohr, respectively, are the result of an avoided crossing at about 4.6 bohr, mainly between two $^3\Delta$ states, the fifth and the 12th, in ascending energy order. The "*l*" minimum traces its ancestry to $|a^4F; M = \pm 2\rangle \otimes |^2P; M = 0\rangle$, with an equilibrium configuration of $5|^3\Delta(^3A_1)\rangle_1 \sim 0.84|1\sigma^2 2\sigma^2 3\sigma^1 1\delta_+^1\rangle$, and CAS atomic populations $4s^{1.09}4p_z^{0.06}3d_{z^2}^{1.03}3d_{x^2-y^2}^{1.0}$/

$2s^{1.85}2p_z^{0.85}2p_x^{0.06}2p_y^{0.06}$. Both the $3d_{z^2}(3\sigma)$ and $3d_{x^2-y^2}(\delta_+)$ electrons have spectator character without any participation in the bonding. Thus at the "*l*" minimum the bonding can be clearly pictured by

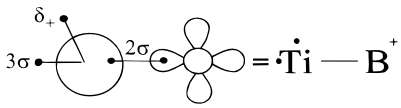

Overall, ~0.20 e^- is transferred from B to Ti^+ via the σ frame.

Now in the "*g*" minimum of the PEC the dominant configurations are

$$5|^3\Delta(^3A_1)\rangle_g \sim 1\sigma^2 2\sigma^1 1\pi_x^1 1\pi_y^1 1\delta_-^1(0.59\alpha\beta\alpha\alpha + 0.55\alpha\alpha\alpha\beta + 0.33\alpha\alpha\beta\alpha) - 0.12|1\sigma^2 2\sigma^1 1\delta_+^1(1\pi_x^2 + 1\pi_y^2)\rangle$$

resulting in a dramatic change of bonding mechanism as compared to the "*l*" minimum. The atomic distributions are

$$4s^{0.25}4p_z^{0.11}3d_{z^2}^{0.31}3d_{xz}^{0.70}3d_{yz}^{0.70}3d_{x^2-y^2}^{0.05}3d_{xy}^{0.95}/2s^{1.52}2p_z^{0.78}2p_x^{0.30}2p_y^{0.30}$$

The in situ metal is in a $d^3(b^4F; M=\pm 2)$ configuration; the $3d_{xy}(\delta_-)$ e^- does not participate in the bonding, while 2×0.30 e^- are transferred from the $3d_\pi$(Ti) to the $2p_\pi$(B) orbitals, creating two half π bonds. Via the strongly hybridized 2s, $2p_z$ orbitals of B ~ 0.7 e^- migrate to the $4s4p_z3d_{z^2}(2\sigma)$ hybrid of the Ti atom. These findings can be captured by the vbL picture

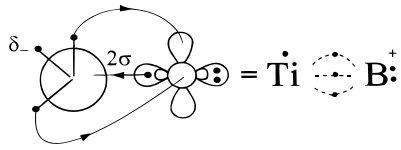

with two half π bonds and a half σ bond. The binding in this $5^3\Delta$ state is identical to that of the $X^5\Delta$ state; the 15 kcal/mol difference in D_e is the result of the different spin coupling between the two states.

$6^3\Gamma$ State (3rd of the Triplets). At equilibrium the prevailing configurations are

$$6|^3\Gamma(^3A_1)\rangle \sim 1\sigma^2 2\sigma^1 1\pi_x^1 1\pi_y^1 1\delta_-^1(0.54\alpha\alpha\beta\alpha - 0.30\alpha\beta\alpha\alpha) - 0.43|1\sigma^2 2\sigma^1 1\delta_+^1(1\pi_x^2 - 1\pi_y^2)\rangle$$

Our CAS reference one-electron basis is not optimum for this symmetry, as resulting from a state-average process on three states of $^3\Delta$ symmetry. Table 3 lists our numerical results, and Figure 4 shows the PEC which correlates to $6|^3\Gamma\rangle = |a^4F; M = \pm 3\rangle \otimes |^2P; M = \pm 1\rangle$ fragments. The inherent multiconfiguration nature of this state renders its visual representation by a vbL illustration difficult.

$8^3\Sigma^-$ State (4th of the Triplets). The PEC shown in Figure 4 presents two minima, a global "*g*" and a local "*l*" at about 5.1 and 3.8 bohr, respectively, due to an avoided crossing. At the "*g*" minimum the dominantly contributing configurations are $8|^3\Sigma^-\rangle_g \sim 0.77|1\sigma^2 2\sigma^2 1\pi_x^1 1\pi_y^1\rangle - 0.39|1\sigma^2 2\sigma^2 1\delta_+^1 1\delta_-^1\rangle$, correlating to $8|^3\Sigma^-\rangle = |a^4F; M = 0\rangle \otimes |^2P; M = 0\rangle$. The equilibrium CAS atomic distributions are

$$4s^{1.10}4p_z^{0.06}3d_{z^2}^{0.04}3d_{xz}^{0.80}3d_{yz}^{0.80}3d_{x^2-y^2}^{0.20}3d_{xy}^{0.20}/2s^{1.84}2p_z^{0.82}2p_x^{0.06}2p_y^{0.06}$$

From the atomic populations it is rather obvious that the bonding character of this state can be pictured by the vbL diagram

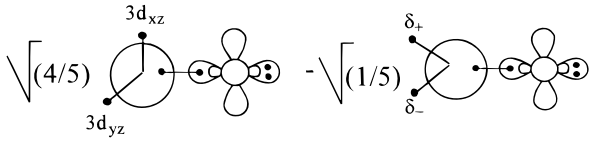

with ~0.20 e^- transferred from B to Ti^+ via the σ frame. The two d densities are spectator electrons along the PEC until the "*g*" minimum, each composed of $0.80(d_{xz}) + 0.20(d_{x^2-y^2})$, and $0.80(d_{yz}) + 0.20(d_{xy})$ e^-, respectively. This $0.80/0.20 = 4/1$ electron allocation of the in situ Ti atom reflects its $M = 0$ projection of the a^4F state at infinity: $\sqrt{4/5}|4s^1 3d_{xz}^1 3d_{yz}^1\rangle + \sqrt{1/5}|4s^1 3d_{x^2-y^2}^1 3d_{xy}^1\rangle$. Certainly the atoms are held together by a single σ bond, but no delocalization of the π density occurs due to the $\sqrt{1/5}|\delta_+\delta_-\rangle$ component.

As the two atoms come closer passing the "*g*" minimum, the character of the wave function changes drastically, becoming $8|^3\Sigma^-\rangle_1 \sim 0.80|1\sigma^2 2\sigma^2 1\pi_x^1 1\pi_y^1\rangle$ with CAS atomic populations as follows:

$$4s^{0.27}4p_z^{0.13}3d_{z^2}^{1.15}3d_{xz}^{0.66}3d_{yz}^{0.66}3d_{x^2-y^2}^{0.10}3d_{xy}^{0.10}/2s^{1.58}2p_z^{0.67}2p_x^{0.31}2p_y^{0.31}$$

Our populations are consistent with the following bonding scheme:

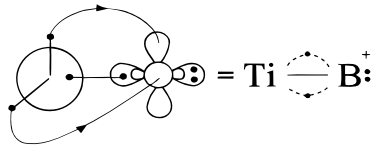

with two half π bonds and a σ bond; overall ~0.13 e^- is transferred from B to Ti via the σ frame. The very abrupt morphological change of the PEC around 3.8 bohr, along with the population allotment, suggests that the metal correlates to a d^3 distribution, namely, $d_{z^2}d_{xz}d_{yz}$. Two atomic Ti^+ states are the *only* candidates carrying the appropriate spatial distribution, the $|b^4F\rangle$ and $|a^4P\rangle$ ~ 0.1 and 1.1 eV above the ground $|a^4F\rangle$ state,[2]

$$|b^4F\rangle = \sqrt{4/5}|3d_{z^2}3d_{x^2-y^2}3d_{xy}\rangle - \sqrt{1/5}|3d_{z^2}3d_{xz}3d_{yz}\rangle$$

$$|a^4P\rangle = \sqrt{4/5}|3d_{z^2}3d_{xz}3d_{yz}\rangle + \sqrt{1/5}|3d_{z^2}3d_{x^2-y^2}3d_{xy}\rangle$$

The interaction of these two atomic states leads to a practical expulsion of the $d_{z^2}d_{x^2-y^2}d_{xy}$ component, rendering the delocalization of the $3d_\pi$ Ti electrons toward the B atom and the creation of two half π bonds possible.

$10^3\Phi$ State (5th of the Triplets). The PEC shown in Figure 4 presents two minima, a "*g*" and a "*l*", differing in energy by less than 2 mhartrees at the MRCI level, Table 3. The dominant configurations (B_1 component) at the "*g*" minimum are given by the combination:

$$10|^3\Phi\rangle_g \sim |1\sigma^2 2\sigma^2 1\delta_+^1 1\pi_x^1\rangle + |1\sigma^2 2\sigma^2 1\pi_y^1 1\delta_-^1\rangle$$

The asymptotic wave function is represented by the product $10|^3\Phi\rangle = |a^4F; M = \pm 3\rangle \otimes |^2P; M = 0\rangle$. At the "*g*" equilibrium the CAS atomic populations are

$$4s^{1.07}4p_z^{0.07}3d_{z^2}^{0.06}3d_{xz}^{0.50}3d_{yz}^{0.50}3d_{x^2-y^2}^{0.50}3d_{xy}^{0.50}/2s^{1.83}2p_z^{0.85}2p_x^{0.06}2p_y^{0.06}$$

The binding mode is succinctly represented by the vbL icon

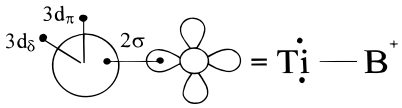

We have a pure σ bond and two spectator symmetry defining electrons (d_π, d_δ) indifferent to the bonding. The bonding mechanism strongly resembles the $2^3\Pi$ state (vide supra); as in that case, $\sim$0.20 e^- is transferred from B to Ti via the σ frame. At the "*g*" minimum the in situ metal mirrors perfectly its asymptotic distribution, as it should, due to the $M = \pm 3$ symmetry commitment.

As we approach the "*l*" minimum around 4 bohr (Figure 4), the electronic milieu transforms drastically. The leading configurations (B_1 component) are $10|^3\Phi\rangle_1 \sim |1\sigma^2 1\delta_+^1 1\pi_x^1 1\pi_y^2\rangle + |1\sigma^2 1\pi_x^2 1\pi_y^1 1\delta_-^1\rangle$, with corresponding CAS populations

$$4s^{0.15}4p_z^{0.09}3d_{z^2}^{0.17}3d_{xz}^{0.82}3d_{yz}^{0.82}3d_{x^2-y^2}^{0.50}3d_{xy}^{0.50}/2s^{1.56}2p_z^{0.09}2p_x^{0.61}2p_y^{0.61}$$

The in situ metal finds itself in its $a^4F(M=\pm 3)$ ground state, with the B atom in its $^4P(M=0)$ first excited state. The bonding is represented by the vbL picture

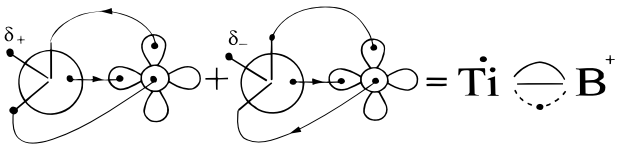

composed of a σ bond, a π bond, and a half π bond; the $\delta_\pm$ density is a spectator electron. In the π frame we have 3 $e^- \sim (0.82 + 0.61) \times 2$ e^-, with 0.6 $e^- = 1 - (0.15 + 0.09 + 0.17)$ transferred from the Ti 4s to the B 2s. Notice the large difference between the bond lengths, 0.7 Å at the MRCI level (Table 3), between the "*g*" and "*l*" minima, reflecting the difference in binding character, a single σ bond vs 2.5 bonds, respectively. Although the binding energy is practically the same for both the "*g*" and "*l*" minima, $\sim$29 kcal/mol (Table 3), the latter has an *internal bond strength*, viz., with respect to $Ti^+(a^4F) + B(^4P)$ products, of 110.4 kcal/mol, not a surprising value for 2.5 bonds.

$11^3\Sigma^+$ State (6th of the Triplets). This is a state very similar to the previously reported $6^3\Gamma$ state, something that can also be seen from its leading configurations,

$$11|^3\Sigma^+\rangle \sim 1\sigma^2 2\sigma^1 1\pi_x^1 1\pi_y^1 1\delta_-^1(0.49\alpha\alpha\beta\alpha - 0.28\alpha\beta\alpha\alpha) + 0.41|1\sigma^2 2\sigma^1 1\delta_+^1(1\pi_x^2 - 1\pi_y^2)\rangle$$

the only difference being the *plus* instead of the *minus* sign in the second term. Exactly the same approach was followed as in the $6^3\Gamma$ state, with the numerical results and the PEC reported in Table 3 and Figure 4; the PEC correlates to $|a^4F; M = \pm 1\rangle \otimes |^2P; M = \mp 1\rangle$.

$12^3\Delta$ State (7th of the Triplets). The PEC shown in Figure 4 presents two minima, the first from the right "*l*" and the second "*g*" at 4.7 and 4.0 bohr, respectively, and an energy difference between them of 6.8 mhartrees. We focus first at the "*l*" minimum with leading configurations

$$12|^3\Delta(^3A_1)\rangle_1 \sim 1\sigma^2 2\sigma^1 1\pi_x^1 1\pi_y^1 1\delta_-^1(0.57\alpha\alpha\alpha\beta + 0.52\alpha\beta\alpha\alpha + 0.30\alpha\alpha\beta\alpha) - 0.12|1\sigma^2 2\sigma^1 1\delta_+^1(1\pi_x^2 + 1\pi_y^2)\rangle$$

and tracing its origin to $12|^3\Delta\rangle = |a^4F; M = \pm 3\rangle \otimes |^2P; M = \mp 1\rangle$. Following the PEC from infinity, at around 5 bohr, a drastic change of configurations is observed as a result of the Ti^+ $d^3(b^4F; M=\pm 2)$ intervention at the "*l*" minimum. Here the dominating presence of the d^3 metal configuration is obvious from the CASSCF atomic populations

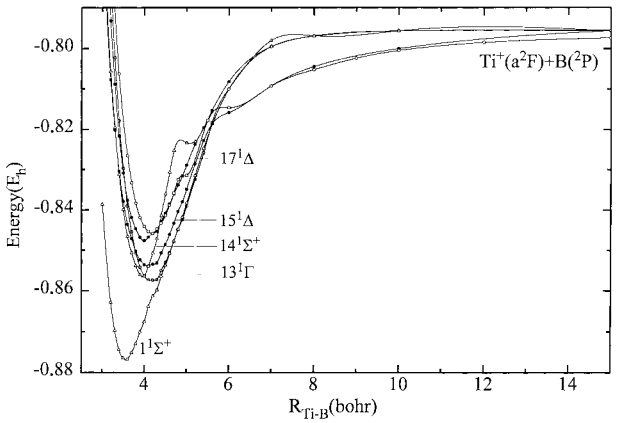

Figure 5. Singlet potential energy curves of $\Sigma^\pm$, Δ, and Γ symmetries; MRCI level of theory.

$$4s^{0.39}4p_z^{0.07}3d_{z^2}^{0.17}3d_{xz}^{0.71}3d_{yz}^{0.71}3d_{x^2-y^2}^{0.06}3d_{xy}^{0.93}/2s^{1.63}2p_z^{0.71}2p_x^{0.29}2p_y^{0.29}$$

leading unequivocally to the following vbL icon

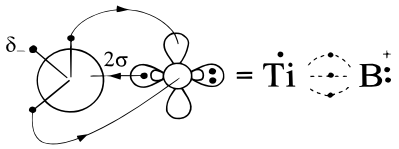

The bonding is due to three half-bonds, one σ and two π, with $\sim$0.6 e^- moving from Ti to the B atom via the π frame and an equal e^- transfer from B to a $4s3d_{z^2}$ hybrid on the Ti atom. The symmetry carrying δ_- density is a spectator electron with no participation in the bonding. This "*l*" $12^3\Delta$ state is "naturally" similar to the "*g*" $5^3\Delta$ state due to the avoided crossing (vide supra), while the observed numerical differences in D_e and R_e are the results of the forced orthogonality between the two states.

The "*g*" minimum has practically the same character as the "*l*", as it appears from the dominant configurations

$$12|^3\Delta(^3A_1)\rangle_g \sim 1\sigma^2 2\sigma^1 1\pi_x^1 1\pi_y^1 1\delta_-^1(0.45\alpha\alpha\alpha\beta - 0.45\alpha\beta\alpha\alpha - 0.26\alpha\alpha\beta\alpha) - 0.39|1\sigma^2 2\sigma^1 1\delta_+^1(1\pi_x^2 + 1\pi_y^2)\rangle$$

The CAS atomic populations at the "*g*" minimum are

$$4s^{0.21}4p_z^{0.11}3d_{z^2}^{0.58}3d_{xz}^{0.57}3d_{yz}^{0.57}3d_{x^2-y^2}^{0.37}3d_{xy}^{0.61}/2s^{1.55}2p_z^{0.53}2p_x^{0.41}2p_y^{0.41}$$

The binding scheme is the same as in the "*l*" case, the only difference being the allotment of the δ spectator electron between the δ_+ and δ_- functions.

4.3 Singlets. We report 11 singlet states, the PECs of which are shown, for reasons of clarity, in Figures 5 ($^1\Sigma^\pm$, $^1\Delta$, $^1\Gamma$) and 6 ($^1\Pi$, $^1\Phi$); numerical results are presented in Table 4.

$1^1\Sigma^+$ State (1st of the Singlets). This is the first excited state lying 8.35 kcal/mol above the ground $X^5\Delta$ state at the MRCI level of theory (Tables 2 and 4). At equilibrium the leading configuration is $\sim 0.90|1\sigma^2 1\pi_x^2 1\pi_y^2\rangle$, with the asymptotic wave function represented by the product

$$1|^1\Sigma^+\rangle = |a^2F; M = \pm 1\rangle \otimes |^2P; M = \mp 1\rangle$$

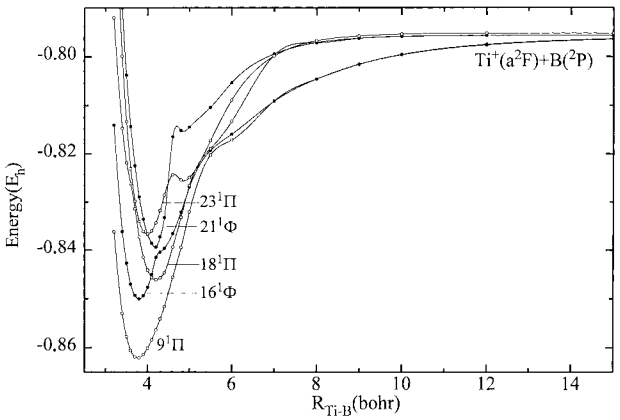

Figure 6. Singlet potential energy curves of Π and Φ symmetries; MRCI level of theory.

Notice that the metal fragment is in its second excited state, as dictated by the spin symmetry. All binding energies (D_e) reported in Table 4 are with respect to the asymptotic products; binding energies with respect to *ground*-state fragments are obtained by substracting the (calculated) 12.1 kcal/mol Ti^+, $a^2F \leftarrow a^4F$ excitation energy.

The CAS equilibrium atomic populations are

$$4s^{0.20}4p_z^{0.11}3d_{z^2}^{0.20}3d_{xz}^{1.27}3d_{yz}^{1.27}/2s^{1.44}2p_z^{0.06}2p_x^{0.68}2p_y^{0.68}$$

suggesting the following binding scheme

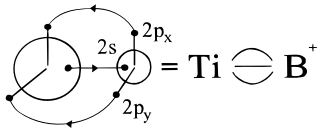

that is, a full triple bond. About 0.5 e^- are transferred from Ti^+ to B through the σ frame with a synchronous transfer of $\sim$0.5 e^- from B to Ti^+ through the π frame. Due to the triple bond the $1^1\Sigma^+$ state has a remarkably short bond length as compared to all other 23 states. For instance, all states characterized by a single σ bond ($2^3\Pi_l$, $5^3\Delta_l$, $8^3\Sigma^-_g$, $10^3\Phi_g$) have a bond length of about 2.7 Å, $\sim$0.8 Å longer than the present state. In Table 4 we report a $D_e = 51.7$ kcal/mol (or $51.7 - 12.1 = 39.6$ kcal/mol with respect to the ground-state atoms), not in congruence with its binding order. However, the *internal bond strength*, that is the binding energy with respect to the *diabatic* products, $Ti^+(a^4F; M{=}0) + B(^4P; M{=}0)$, is 120 kcal/mol, reflecting the triple-bond character of the $1^1\Sigma^+$ state. That the in situ B atom finds itself in the ^4P is clearly suggested by the equilibrium electron distributions: the $2p_z$ function carries only 0.06 e^- (its GVB correlation), with 1.95 e^- allotted among the $2s + 4s4p_z3d_{z^2}$ orbitals, while the remaining 2 e^- of B are distributed in the π frame, $2(0.68 + 0.27)$. It is revealing to constrast the binding mechanism of this state with the ground $^1\Sigma^+$ states of the isovalent triple-bonded species Ti≡N^{+19} and Ti≡C−H^+.[20] For these molecules the D_e's and R_e's are 120 kcal/mol, 1.586 Å ($Ti^+(a^4F) + N(^4S)$) and 113 kcal/mol, 1.758 Å ($Ti^+(a^4F) + CH(^4\Sigma^-)$), with corresponding experimental D_e values of 116.3 ± 2.8[21] and 114.2 ± 1.3[22] kcal/mol, respectively.

$9^1\Pi$ State (2nd of the Singlets). The equilibrium configurations for this state are

$$9|^1\Pi(^1B_1)\rangle \sim 0.75|1\sigma^2 2\sigma^1 1\bar{\pi}_x^1 1\pi_y^2\rangle - 0.22(|1\sigma^2 1\delta_+^1 1\bar{\pi}_x^1 1\pi_y^2\rangle + |1\sigma^2 1\pi_x^2 1\pi_y^1 1\bar{\delta}_-^1\rangle)$$

with the asymptotic wave function given by the product $9|^1\Pi\rangle = |a^2F; M = \pm1\rangle \otimes |^2P; M = 0\rangle$. The PEC presented in Figure 6 is the result of three strongly interacting $^1\Pi$ states, all shown in Figure 6. Around 5 bohr the mixing of the three $^1\Pi$ states gives rise to a switching of the asymptotic M values $Ti^+(M{=}0)$, $B(M{=}\pm1)$, while around 4.5 bohr an avoided crossing between the third of the $^1\Pi$ states ($23^1\Pi$) and a fourth $^1\Pi$ state (not shown in Figure 6) of the Ti^+ $d^3(a^2G)$ distribution is responsible for introducing the 0.22 component (d^3) in the leading equilibrium configurations previously mentioned. The CAS atomic populations are

$$4s^{0.24}4p_z^{0.11}3d_{z^2}^{0.54}3d_{xz}^{0.71}3d_{yz}^{1.16}3d_{x^2-y^2}^{0.11}3d_{xy}^{0.11}/2s^{1.50}2p_z^{0.46}2p_x^{0.32}2p_y^{0.66}$$

Taking into account only the "0.75" component of the leading configurations, the nature of the bonding can be more or less represented by the vbL icon

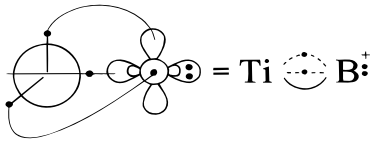

implying a π bond, a half π bond, and a half σ bond, with no net charge transfer from one atom to the other. Our populations suggest that the in situ Ti atom is a linear combination of two, $M = 0$, configurations,

$$|0\rangle = \sin\varphi|(4s3d^2), b^2F; M = 0\rangle + \cos\varphi|(3d^3), a^2G; M = 0\rangle$$

Although the π-bonding character cannot be questioned, the σ interaction is rather ambiguous; we can only ascertain a strong $(sp_z)^{2.0}$ hybridization on the B atom with 3 e^- entailed in the σ frame of the system.

$13^1\Gamma$ State (3rd of the Singlets). This is not an easily analyzable state due to the large number of significantly contributing configurations in the CASSCF wave function. For instance, some of the main contributing configurations are

$$13|^1\Gamma(^1A_1)\rangle \sim 1\sigma^2 2\sigma^1 1\pi_x^1 1\pi_y^1 1\delta_-^1(0.31\alpha\beta\alpha\beta + 0.53\alpha\alpha\beta\beta) + 0.43|1\sigma^2 2\sigma^1 1\bar{\delta}_+^1(1\pi_x^2 + 1\pi_y^2)\rangle$$

with the asymptotic wave function being

$$13|^1\Gamma\rangle = |a^2F; M = \pm3\rangle \otimes |^2P; M = \pm1\rangle$$

The equilibrium atomic CAS populations are

$$4s^{0.36}4p_z^{0.13}3d_{z^2}^{0.26}3d_{xz}^{0.63}3d_{yz}^{0.63}3d_{x^2-y^2}^{0.50}3d_{xy}^{0.50}/2s^{1.46}2p_z^{0.77}2p_x^{0.36}2p_y^{0.36}$$

The vbL representation of the bonding (A_1 component) can be written as

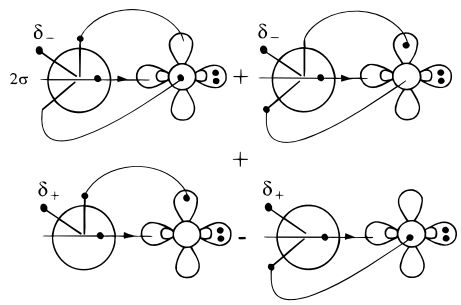

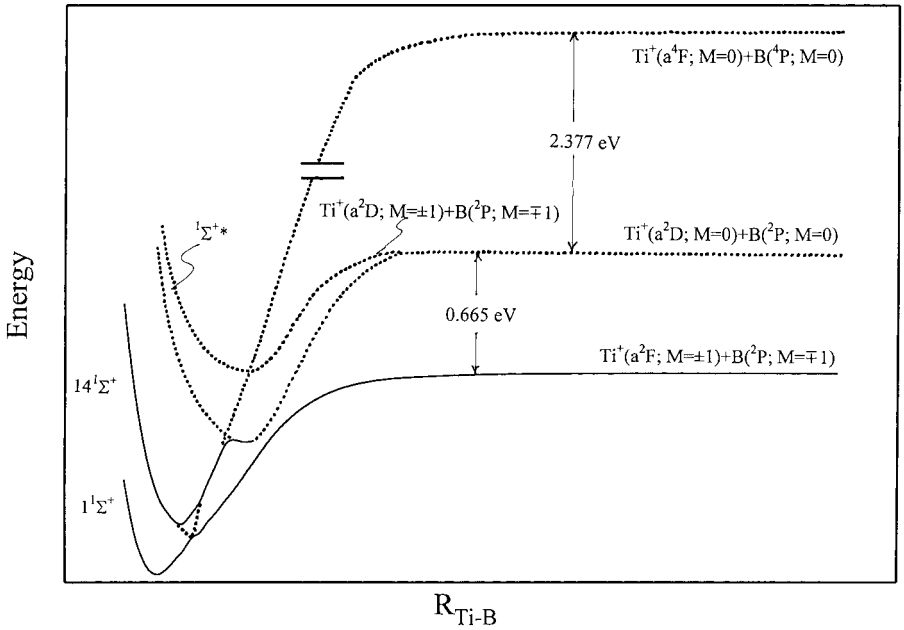

Figure 7. Schematic representation (not in scale) of the $^1\Sigma^+$ interacting manifold. Dotted curves have not been calculated.

with corresponding pictures for the A_2 component. The presence of a $2p_x$ or $2p_y$ electron on the B atom, not obvious from the population distributions, is dictated by its $M = \pm 1$ value due to the $\Gamma(|\Lambda| = 4)$ symmetry. Grossly speaking, we can claim that the bonding is comprised of a π bond and a half σ bond. In the σ frame 0.25 e^- is transferred from the $(4s4p_z\text{-}3d_{z^2})^{1.0}$ hybrid to the $(sp_z)^{2.0}$ hybrid on the B atom, while via the π frame about 0.25 e^- is transferred to the metal, so no net charge movement is found.

$14^1\Sigma^+$ State (4th of the Singlets). This is the only state that correlates to the a^2D state of the Ti^+ cation. The CASSCF wave function contains a multitude of significantly contributing configurations with coefficients of 0.2−0.3, so no "simple" interpretation of the bonding character is possible. At infinity, the wave function is given by the product $|a^2D; M = 0\rangle \otimes |^2P; M = 0\rangle$. In the PEC shown in Figure 5 a global minimum is observed around 3.9 bohr, while at about 5.4 bohr a local minimum appears, not clearly discerned at the MRCI PEC, reflecting the asymptotic character (a^2D; M=0) of the metal. For purely technical reasons we were unable to compute the 5.2 bohr-to-infinity PEC.

To further clarify the situation here, in Figure 7 we present a schematic (partial) drawing of the PECs involved; the dotted part of the curves has not been calculated. The left (repulsive) part of the $14^1\Sigma^+$ PEC is dominated by the asymptotic character of the $1^1\Sigma^+$ state. The right part, and in particular, between 3.7 and 5.0 bohr (overlaping curves), is controlled by the asymptotic diabatic (dotted curve) part of the $1^1\Sigma^+(a^4F; M=0 + {}^4P; M=0)$ state, thus transmitting the triple-bond character of this state (vide supra) to the $14^1\Sigma^+$ state. Therefore, the equilibrium character of the $14^1\Sigma^+$ state is a *melange* due to the avoided crossing between the *diabatic* curves $1^1\Sigma^+ \rightarrow Ti^+(a^4F; M=0) + B(^4P; M=0)$ and the $14^1\Sigma^+ \rightarrow Ti^+(a^2F; M=\pm1) + B(^2P; M=\mp1)$. The $D_e = 52.8$ kcal/mol reported in Table 4 is with respect to $Ti^+(a^2D; M=0) + B(^2P; M=0)$. To obtain the dissociation energy with respect to ground-state products, the calculated excitation energy $Ti^+(a^2D \leftarrow a^4F)$ of 27.5 kcal/mol should be substracted from the 52.8 kcal/mol value. Now, the *internal bond strength* of the $14^1\Sigma^+$ state is calculated with respect to the $Ti^+(a^2F; M=\pm1) + B(^2P; M=\mp1)$ asymptote, or 38.5 kcal/mol. For reasons of completeness a $^1\Sigma^{+*}$ *diabatic* state (dotted line) is schematically drawn (not calculated) in Figure 7, correlating to $Ti^+(^2D; M=\pm1) + B(^2P; M=\mp1)$ fragments.

The equilibrium CAS atomic populations, admittedly not very revealing, are $4s^{0.27}4p_z^{0.13}3d_{z^2}^{0.58}3d_{xz}^{0.72}3d_{yz}^{0.72}3d_{x^2-y^2}^{0.29}3d_{xy}^{0.29}/2s^{1.48}2p_z^{0.63}2p_x^{0.41}2p_y^{0.41}$, with no net charge transfer.

$15^1\Delta$ State (5th of the Singlets). The PEC shown in Figure 5 correlates to $Ti^+(a^2F; M=\pm2) + B(^2P; M=0)$ asymptotic products. As we trace the potential curve to the left, a strong interaction occurs around 5.5 bohr among the three $^1\Delta$ states correlating to $Ti^+(a^2F; M=\pm1,\pm2,\pm3) + B(^2P; M=\pm1,0,\mp1)$. At equilibrium (2.18 Å, Table 4), the CAS wave function does not contain a dominant configuration and is composed of a large number of significantly contributing configurations. For instance, the largest contributions to the A_1 component are

$$15|^1\Delta(^1A_1)\rangle \sim 0.52|1\sigma^2 2\sigma^1 1\bar{\delta}_+^1(1\pi_x^2 + 1\pi_y^2)\rangle + 0.22|1\sigma^2 2\sigma^1 3\bar{\sigma}^1(1\pi_x^2 - 1\pi_y^2) + 0.20|1\sigma^2 2\sigma^2(1\pi_x^2 - 1\pi_y^2)\rangle - 0.12|1\sigma^2 2\sigma^1 1\bar{\pi}_x^1 1\pi_y^1 1\bar{\delta}_-^1\rangle$$

The corresponding CAS-atomic populations are

$$4s^{0.34}4p_z^{0.14}3d_{z^2}^{0.50}3d_{xz}^{0.63}3d_{yz}^{0.63}3d_{x^2-y^2}^{0.74}3d_{xy}^{0.03}/2s^{1.45}2p_z^{0.77}2p_x^{0.36}2p_y^{0.36}$$

While two half π bonds can be clearly discerned, no simple picture can be given for the σ and $\delta_\pm$ interactions.

$16^1\Phi$ State (6th of the Singlets). The asymptotic wave function is represented by the product $|a^2F; M = \pm3\rangle \otimes |^2P; M = 0\rangle$, with the following leading equilibrium configuration:

$$16|^1\Phi(^1B_1)\rangle \sim 0.62(|1\sigma^2 1\delta_+^1 1\bar{\pi}_x^1 1\pi_y^2\rangle - |1\sigma^2 1\pi_x^2 1\pi_y^1 1\bar{\delta}_-^1\rangle)$$

The PEC shown in Figure 6 presents an avoided crossing around 4.2 bohr with the $21^1\Phi$ state, lying some 7 kcal/mol above the $16^1\Phi$ state (Figure 2). Close to equilibrium the $21^1\Phi$ state lends its character to the $16^1\Phi$ due to the avoided crossing. However, the character of the $21^1\Phi$ state originates from an avoided crossing at about 4.6 bohr (Figure 5) between this state and another $^1\Phi$ tracing its *diabatic* origin to $Ti^+(a^4F; M=\pm3) + B(^4P; M=0)$ fragments. The equilibrium CAS atomic distribu-

tions of this state are

$$4s^{0.17}4p_z^{0.09}3d_{z^2}^{0.19}3d_{xz}^{0.76}3d_{yz}^{0.76}3d_{x^2-y^2}^{0.50}3d_{xy}^{0.50}/2s^{1.50}2p_z^{0.09}2p_x^{0.68}2p_y^{0.68}$$

leading to the following vbL bonding icon

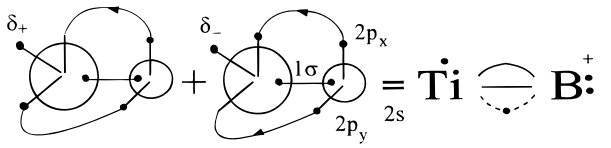

with a σ bond, a π bond, and a half π bond; notice the ^{4}P character of the in situ B atom. In the σ frame 0.5 e^- from the $(4s4p_z3d_{z^2})^{1.0}$ hybrid are transferred to the $2s^{1.0}$ boron orbital, giving rise to a pure σ bond. In the π frame $0.6 \sim 2(1 - 0.68)$ e^- are transferred from the B to the Ti atom, so no net charge transfer occurs. The δ frame hosts one spectator electron. The almost triple-bond character is reflected in the short bond length (2.010 Å, Table 4) of this state, almost the shortest among the excited singlets. While the D_e value with respect to the asymptotic products is 34.7 kcal/mol, the *internal bond strength*, namely with respect to $Ti^+(a^4F) + B(^4P)$, is 105 kcal/mol.

17$^1\Delta$ State (7th of the Singlets). The equilibrium leading configurations are

$$17|^1\Delta(^1A_1)\rangle \sim 1\sigma^2 2\sigma^1 1\pi_x^1 1\pi_y^1 1\delta_-^1(0.63\alpha\beta\alpha\beta + 0.37\alpha\alpha\beta\beta) + 0.20|1\sigma^2 2\sigma^2(1\pi_x^2 - 1\pi_y^2)\rangle$$

The PEC curve is shown in Figure 5 correlating to the product wave function, $|a^2F;\ M = \pm 3\rangle \otimes |^2P;\ M = \mp 1\rangle$. The CAS atomic populations

$$4s^{0.26}4p_z^{0.12}3d_{z^2}^{0.64}3d_{xz}^{0.56}3d_{yz}^{0.56}3d_{x^2-y^2}^{0.02}3d_{xy}^{0.81}/2s^{1.51}2p_z^{0.60}2p_x^{0.42}2p_y^{0.42}$$

suggest the following bonding scheme:

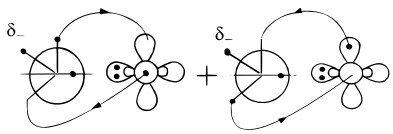

The bonding is composed mainly of two half π bonds, with essentially no bonding interaction along the σ frame and the δ_- density being a spectator electron.

18$^1\Pi$ State (8th of the Singlets). The PEC of this state (Figure 6) traces its lineage to the atomic states $Ti^+(a^2F;\ M{=}\pm 2) + B(^2P;\ M{=}\mp 1)$. At equilibrium the most important contributions are

$$18|^1\Pi(^1B_1)\rangle \sim 0.48(|1\sigma^2 2\sigma^2 1\pi_y^1 1\bar{\delta}_-^1\rangle + |1\sigma^2 2\sigma^2 1\delta_+^1 1\bar{\pi}_x^1\rangle) - 0.24(|1\sigma^2 2\sigma^{*2} 1\pi_y^1 1\bar{\delta}_-^1\rangle + |1\sigma^2 2\sigma^{*2} 1\delta_+^1 1\bar{\pi}_x^1\rangle)$$

not an easily interpreted state, as is also evident from the CAS equilibrium atomic populations

$$4s^{0.42}4p_z^{0.14}3d_{z^2}^{1.07}3d_{xz}^{0.16}3d_{yz}^{0.20}3d_{x^2-y^2}^{0.50}3d_{xy}^{0.50}/2s^{1.49}2p_z^{0.75}2p_x^{0.48}2p_y^{0.38}$$

As in previouly reported states, the very large number of significantly contributing configurations betrays a simple "chemical" bonding interpretation.

20$^1\Sigma^-$ State (9th of the Singlets). At infinity, the PEC of this $20^1\Sigma^-$ state (Figure 5) correlates to $Ti^+(a^2F;\ M = 0)$+B-$(^2P;\ M = 0)$. As we approach the equilibrium, and around 5 bohr, an avoided crossing with a $^1\Sigma^-$ state tracing its origin to $Ti^+(a^2F;\ M = \pm 1)$+B(^{2}P; M = $\mp$1), occurs. As a result the two PECs interchange their character by switching their M values. At equilibrium (4.20 bohr) the leading configurations are

$$20|^1\Sigma^-\rangle \sim 0.32|1\sigma^2 2\sigma^1 3\sigma^1 1\bar{\pi}_x^1 1\bar{\pi}_y^1\rangle + 0.55|1\sigma^2 2\sigma^1 1\bar{\delta}_+^1 1\pi_x^1 1\bar{\pi}_y^1\rangle - 0.39|1\sigma^2 2\sigma^1 1\bar{\delta}_-^1(1\pi_x^2 - 1\pi_y^2)\rangle$$

The $|M = \pm 1\rangle \otimes |M = \mp 1\rangle$ asymptote in terms of atomic functions is composed of the following leading terms:

$$\sim 0.38(|4s3\bar{d}_{z^2}3d_{xz}2\bar{p}_y\rangle - |4s3\bar{d}_{z^2}2p_x3\bar{d}_{yz}\rangle) + 0.33(|4s3\bar{d}_{xz}2p_x3\bar{d}_{xy}\rangle - |4s3\bar{d}_{yz}2p_y3\bar{d}_{xy}\rangle) + 0.32(|4s3\bar{d}_{x^2-y^2}3d_{xz}2\bar{p}_y\rangle + |4s3\bar{d}_{x^2-y^2}3d_{yz}2\bar{p}_x\rangle)$$

clearly reflecting the equilibrium structure of this state and ascertaining the avoided crossing. Our 4.2 bohr CAS atomic populations are

$$4s^{0.47}4p_z^{0.09}3d_{z^2}^{0.33}3d_{xz}^{0.63}3d_{yz}^{0.63}3d_{x^2-y^2}^{0.41}3d_{xy}^{0.41}/2s^{1.50}2p_z^{0.75}2p_x^{0.35}2p_y^{0.35}$$

While the σ bonding mode is rather obscure, it is clear that we have two half π bonds and a nonbonding $\delta_\pm$ electron, with no total charge transfer between the two atoms.

21$^1\Phi$ State (10th of the Singlets). The PEC shown in Figure 6 correlates to $Ti^+(a^2F;\ M{=}\pm 2) + B(^2P;\ M{=}\pm 1)$, but around 4.6 bohr an avoided crossing intervenes with a $^1\Phi$ state tracing its origin to $Ti^+(a^4F;\ M{=}\pm 3) + B(^4P;\ M{=}0)$ (see also the $16^1\Phi$ discussion). Around equilibrium (4.2 bohr), the present state interacts strongly with the $16^1\Phi$ state; thus the leading equilibrium CAS configurations,

$$21|^1\Phi(^1B_1)\rangle \sim 0.45(|1\sigma^2 2\sigma^2 1\pi_y^1 1\bar{\delta}_-^1\rangle + |1\sigma^2 2\sigma^2 1\delta_+^1 1\bar{\pi}_x^1\rangle) - 0.20(|2\sigma^2 1\delta_+^1 1\bar{\pi}_x^1 1\pi_y^2\rangle - |2\sigma^2 1\pi_x^2 1\pi_y^1 1\bar{\delta}_-^1\rangle)$$

mirror two asymptotes: The "0.45" contribution correlates to $Ti^+(a^2F;\ M{=}\pm 3) + B(^2P;\ M{=}0)$, and the "0.20" to $Ti^+(a^4F;\ M{=}\pm 3) + B(^4P;\ M{=}0)$ asymptote. The CAS atomic populations are

$$4s^{0.42}4p_z^{0.14}3d_{z^2}^{1.0}3d_{xz}^{0.21}3d_{yz}^{0.21}3d_{x^2-y^2}^{0.50}3d_{xy}^{0.50}/2s^{1.47}2p_z^{0.69}2p_x^{0.40}2p_y^{0.40}$$

Certainly, no way to interpret the binding mode using simple pictures is possible due to the particular avoided crossings encountered in this state.

23$^1\Pi$ State (11th of the Singlets). This is the highest of the excited states presented in this report, lying 34.3 kcal/mol above the ground $X^5\Delta$ state. The potential curve shown in Figure 6 shows two minima, a local "*l*" and a global "*g*" around 4.8 and 4.0 bohr, respectively, and correlating to $Ti^+(a^2F;\ M{=}0) + B(^2P;\ M{=}\pm 1)$ atoms. The "*l*" minimum owes its existence to the strong interaction of three $^1\Pi$ states correlating to Ti^+-$(M{=}0,\pm 1,\pm 2) + B(M{=}\pm 1,0,\mp 1)$. The leading configurations at the "*g*" minimum are

$$23|^1\Pi(^1B_1)\rangle_g \sim -0.45(|1\sigma^2 1\delta_+^1 1\bar{\pi}_x^1 1\pi_y^2\rangle + |1\sigma^2 1\pi_x^2 1\pi_y^1 1\bar{\delta}_-^1\rangle) + 0.18(|1\sigma^2 2\sigma^2 1\pi_y^1 1\bar{\delta}_-^1\rangle + |1\sigma^2 2\sigma^2 1\delta_+^1 1\bar{\pi}_x^1\rangle) + 0.31|1\sigma^2 2\sigma^1 1\bar{\pi}_x^1 1\pi_y^2\rangle$$

At about 4.6 bohr an avoided crossing due to a $^1\Pi$ state correlating to $Ti^+(a^4F;\ M{=}\pm 1) + B(^4P;\ M{=}0)$ gives rise to the "0.45" contribution, similar to the "0.20" contribution of the previously discussed $21^1\Phi$ state; the sign change is the result

of spatial symmetry. The "0.18" contribution comes from the $Ti^+(a^2F; M=\pm2) + B(^2P; M=\mp1)$ asymptote, while the "0.31" contribution originates from the $Ti^+(a^2F; M=0) + B(^2P; M=\pm1)$ fragments, the asymptotic products of the $23^1\Pi$ state. As is expected, the equilibrium CAS atomic populations

$$4s^{0.29}4p_z^{0.11}3d_{z^2}^{0.32}3d_{xz}^{0.60}3d_{yz}^{0.76}3d_{x^2-y^2}^{0.44}3d_{xy}^{0.44}/2s^{1.49}2p_z^{0.31}2p_x^{0.51}2p_y^{0.60}$$

are not particularly enlightening due to the complexity of the state.

5. Synopsis and Final Remarks

Using multireference methods (CASSCF+1+2) and relatively large basis sets, we have calculated the ground ($X^5\Delta$) and 23 excited states ($\Sigma^{\pm}$, Π, Δ, Φ, and Γ symmetries) of the six valence electron system TiB^+. For all states we report absolute energies, dissociation energies, bond lengths, harmonic frequencies, energy gaps, and full potential energy curves. In addition, an effort has been made to decipher the bonding mechanisms using simple valence-bond-like pictures.

Within the Born−Oppenheimer Coulombic *ansatz* the accuracy of our results, and in particular D_e values, are affected by uncertainties caused by (a) basis set incompleteness; (b) valence correlation energy losses intrinsic to the MRCISD methodology; (c) size nonextensivity effects; (d) core−valence interactions; and (e) use of "internal contraction" and "state average" techniques.

Our basis set size can be considered as adequate enough judging from the Ti^+ and B atoms' SCF energies as compared to numerical results, the differencies being 0.4 and 0.9 mhartree, respectively (Table 1). Therefore, and taking into account our previous experience, we can claim that the present work is practically free from differential errors due to the basis set size. The combined effect of (b) and (c) can be estimated from the multireference Davidson correction mirrored in the D_e values, which on the average are about 1.5 kcal/mol (Tables 2, 3, 4). For the present work the main effect of (d) is in the atomic energy splitting $a^2F \leftarrow a^4F$, which in turn affects the energy levels of all the singlets because they correlate to $Ti^+(a^2F) + B(^2P)$. The calculated splitting is *underestimated* by 0.9 kcal/mol (Table 1); therefore all singlet PECs should be shifted upward by an equal amount. As a result, the relative ordering of the $9^1\Pi$ and $18^1\Pi$ states will probable change. Both internal contraction and state-average techniques (e) influence the D_e values by about 1 kcal/mol, as already mentioned in section 2. Over all we could ascertain that our MRCI D_e values are underestimated by no more than 2.5 kcal/mol, or an average error of about 5%.

Our main results can be synopsized as follows.

1. All calculated states are bound with respect to the ground-state products, with D_e's ranging from 47.6($X^5\Delta$) to 13.8($23^1\Pi$) kcal/mol at the MRCI level. Mutatis mutandis, the $X^5\Delta$ is isomorphic to the ground, $X^4\Sigma^-$ state of the ScB^+ system.[5]

2. The first excited state, lying 8.3 kcal/mol above the $X^5\Delta$ state, is a "genuinely" triple-bonded $^1\Sigma^+$ state that is perfectly described by a GVB wave function. This is rather obvious from the CASSCF vs MRCI D_e values, 48.9 and 51.7 kcal/mol, respectively. The internal bond strength of this state, $TiB^+ \rightarrow Ti^+(a^4F) + B(^4P)$, is 120.0 kcal/mol, the highest of all states.

3. For the triplets, $2^3\Pi_l$, $5^3\Delta_l$, $8^3\Sigma^-_g$, and $10^3\Phi_g$, where the binding can be unequivoqually described by a pure σ bond, all the D_e values are about 28 kcal/mol and the bond distances around 2.7 Å. The same behavior is observed for the purely σ-bonded states of ScB^+, $^2\Pi_l$, $^2\Delta_l$, and $^2\Sigma^+_g$ where the D_e's are 28.1, 27.2, and 24.6 kcal/mol, respectively.[5]

4. In all states studied, the in situ B atom finds itself significantly promoted in its ^4P excited state; this is very pronounced in the $1^1\Sigma^+$, $10^3\Phi_l$, $16^1\Phi$, and $19^5\Delta$ states.

5. Finally, it is obvious, that we cannot be sure of the ordering of certain states, namely, those that are practically degenerate at the MRCI level. This is most dramatically illustrated for the group of $8^3\Sigma^-$, $9^1\Pi$, $10^3\Phi$, $11^3\Sigma^+$, and $12^3\Delta$ states, which span an energy range of less than 1 mhartree (Figure 2); the $+Q$ Davidson correction completely reshuffles their MRCI ordering within a ~2 mhartree energy range. Also, the $+Q$ correction inverts the ordering of the $4^5\Sigma^-$, $5^3\Delta$ and $19^5\Delta$, $20^1\Sigma^-$ states, differing by just 0.2 and 0.4 mhartree at the MRCI level.

References and Notes

(1) (a) *Quantum Chemistry: The Challenge of Transition Metals and Coordination Chemistry*; Veillard, Ed.; NATO ASI; 1985. (b) Veillard, A. *Chem. Rev.* **1991**, *91*, 743.

(2) Moore, C. E. *Atomic Energy Levels*; NSRDS-NBS Circular No. 35; U.S. GPO: Washington, DC, 1971.

(3) Langhoff, S. R.; Bauschlicher, C. W., Jr. *Annu. Rev. Phys. Chem.* **1988**, *39*, 213.

(4) See for instance the review article by Harrison, J. F.; Kunze, K. L. *Organometallic Ion Chemistry*; Freiser, B. S., Ed.; Kluwer Academic Publishers: Dordrecht, 1996, and references therein, in particular collected refs 1−6.

(5) Kalemos, A.; Mavridis, A. *Adv. Quantum Chem.*, in press.

(6) Bauschlicher, C. W., Jr. *Theor. Chim. Acta* **1995**, *92*, 183.

(7) Dunning, T. H., Jr. *J. Chem. Phys.* **1989**, *90*, 1007.

(8) Bartlett, R. J. *Annu. Rev. Phys. Chem.* **1981**, *32*, 359.

(9) Duch, W.; Diercksen, G. H. F. *J. Chem. Phys.* **1994**, *101*, 3018.

(10) Werner, H.-J.; Knowles, P. J. *J. Chem. Phys.* **1988**, *89*, 5803. Knowles, P. J.; Werner, H.-J. *Chem. Phys. Lett.* **1988**, *145*, 514; Werner, H.-J.; Reinsch, E. A. *J. Chem. Phys.* **1982**, *76*, 3144. Werner, H.-J. *Adv. Chem. Phys.* **1987**, *LXIX*, 1.

(11) Docken, K.; Hinze, J. *J. Chem. Phys.* **1972**, *57*, 4928.

(12) Werner, H.-J.; Meyer, W. *J. Chem. Phys.* **1981**, *74*, 5794.

(13) MOLPRO is a package of ab initio programs written by H.-J. Werner and P. J. Knowles, with contributions from J. Almlof, R. D. Amos, A. Berning, M. J. O. Deegan, F. Eckert, S. T. Elbert, C. Hambel, R. Lindh, W. Meyer, A. Nicklass, K. Peterson, R. Pitzer, A. J. Stone, P. R. Taylor, M. E. Mura, P. Pulay, M. Schuetz, H. Stoll, T. Thorsteinsson, and D. L. Cooper.

(14) Shepard, R.; Shavitt, I.; Pitzer, R. M.; Comeau, D. C.; Pepper, M.; Lischka, H.; Szalay, P. G.; Ahlrichs, R.; Brown, F. B.; Zhao, J.-G. *Int. J. Quantum Chem.* **1988**, *S22*, 149.

(15) (a) Hay, J. *J. Chem. Phys.* **1977**, *66*, 4377. (b) Koga, T.; Tatewaki, H.; Thakkar. A. J. *J. Chem. Phys.* **1994**, *100*, 8140.

(16) Partridge, H. *J. Chem. Phys.* **1989**, *90*, 1043.

(17) Roothaan, C. C. J. *Rev. Mod. Phys.* **1951**, *23*, 69.

(18) Blomberg, M. R. A.; Sieghbahn, P. E. M. *J. Chem. Phys.* **1983**, *78*, 5682.

(19) Kunze, K. L.; Harrison, J. F. *J. Phys. Chem.* **1989**, *93*, 2983.

(20) Mavridis, A.; Alvarado-Swaisgood, E.; Harrison, J. F. *J. Phys. Chem.* **1986**, *90*, 2584.

(21) Clemmer, D. E.; Sunderlin, L. S.; Armentrout, P. B. *J. Phys. Chem.* **1990**, *94*, 3008.

(22) Sunderlin, L. S.; Armentrout, P. B. *J. Phys. Chem.* **1988**, *92*, 1209.